

# The Origin of Disks and Spheroids in Simulated Galaxies

Laura V. Sales<sup>1</sup>, Julio F. Navarro<sup>2</sup>, Tom Theuns<sup>3,4</sup>, Joop Schaye<sup>5</sup>, Simon D. M. White<sup>1</sup>, Carlos S. Frenk<sup>3</sup>, Robert A. Crain<sup>5</sup> and Claudio Dalla Vecchia<sup>6</sup>

<sup>1</sup> Max Planck Institute for Astrophysics, Karl-Schwarzschild-Strasse 1, 85740 Garching, Germany

<sup>2</sup> Department of Physics and Astronomy, University of Victoria, Victoria, BC V8P 5C2, Canada

<sup>3</sup> Institute for Computational Cosmology, Department of Physics, University of Durham, South Road, Durham, DH1 3LE, UK

<sup>4</sup> Department of Physics, University of Antwerp, Campus Groenenborger, Groenenborgerlaan 171, B-2020 Antwerp, Belgium

<sup>5</sup> Leiden Observatory, Leiden University, PO Box 9513, 2300 RA Leiden, Netherlands

<sup>6</sup> Max Planck Institute for Extraterrestrial Physics, Giessenbachstrae 1, 85748 Garching, Germany

13 December 2011

## ABSTRACT

The major morphological features of a galaxy are thought to be determined by the assembly history and net spin of its surrounding dark halo. In the simplest scenario, disk galaxies form predominantly in halos with high angular momentum and quiet recent assembly history, whereas spheroids are the slowly-rotating remnants of repeated merging events. We explore these assumptions using one hundred systems with halo masses similar to that of the Milky Way, identified in a series of cosmological gasdynamical simulations: the Galaxies - Inter-galactic Medium Calculation (GIMIC). At  $z = 0$ , the simulated galaxies exhibit a wide variety of morphologies, from dispersion-dominated spheroids to pure disk galaxies. Surprisingly, these morphological features are very poorly correlated with their halo properties: disks form in halos with high and low net spin, and mergers play a negligible role in the formation of spheroid stars, most of which form in-situ. With hindsight, this weak correlation between halo and galaxy properties is unsurprising given the small fraction of the available baryons ( $\sim 40\%$ ) that end up in galaxies. More important to morphology is the *coherent alignment of the angular momentum* of baryons that accrete over time to form a galaxy. Spheroids tend to form when the spin of newly-accreted gas is misaligned with that of the extant galaxy, leading to the episodic formation of stars with different kinematics that cancel out the net rotation of the system. Disks, on the other hand, form out of gas that flows in with similar angular momentum to that of earlier-accreted material. Gas accretion from a hot corona thus favours disk formation, whereas gas that flows “cold”, often along separate, misaligned filaments, favours the formation of spheroids. In this scenario, most spheroids consist of superpositions of stellar components with distinct kinematics, age, and metallicity, an arrangement that might survive to the present day given the paucity of major mergers. Since angular momentum is acquired largely at turnaround, morphology is imprinted early by the interplay of the tidal field and the shape of the material destined to form the galaxy.

**Key words:** Galaxy: disk – Galaxy: formation – Galaxy: kinematics and dynamics – Galaxy: structure

## 1 INTRODUCTION

Galaxies exhibit a spectacular variety of morphologies, from spheroids to disks to bars to peculiar galaxies of irregular shape. Many physical properties, such as gas content, average stellar age, and the rate of current star formation, are known to correlate with morphology. Of such properties, the one that seems most tractable from a theoretical perspective is the relative importance of organized rotation in the structure of a galaxy. This is commonly referred to as the disk-to-spheroid ratio, since stellar disks are

predominantly rotationally-flattened structures whereas spheroids have shapes largely supported by velocity dispersion.

Since Hubble (1926) published his original morphological classification scheme, our understanding of the provenance of these two defining features of galaxy morphology has been constantly evolving. Spheroids were once thought to originate in the swift transformation of an early-collapsing, non-rotating cloud of gas into stars (Eggen et al. 1962; Partridge & Peebles 1967; Larson 1974), whereas disks were envisioned to result from the collapse of clouds with high angular momentum and inefficient star formation

(Eggen et al. 1962; Larson 1976). The role of mergers as a possible transformational mechanism was championed by Toomre (1977) and gained momentum as the hierarchical nature of structure (and hence, galaxy) formation became accepted (White & Rees 1978; Frenk et al. 1985).

Further development of these ideas led to a broad consensus where disks are thought to form at the center of dark matter halos as a consequence of angular momentum conservation during the dissipational collapse of gas (Fall & Efstathiou 1980; Mo et al. 1998), whereas spheroids result predominantly from merger events (see, e.g., Cole et al. 2000, and references therein). Morphology is thus a transient feature of the hierarchical formation of a galaxy: a disk galaxy may be transformed into a spheroidal one after a major merger, but could then re-form a disk through further gas accretion only to be later disrupted again by another merger. Early galaxy formation simulations gave a visually-compelling demonstration of this scenario, galvanizing support for it (see, e.g., Steinmetz & Navarro 2002).

This consensus view has been broadly implemented in semi-analytic models of galaxy formation, where the properties of galaxies are deduced directly from the physical properties and assembly history of their surrounding halos (see, e.g., Croton et al. 2006; Bower et al. 2006; Somerville et al. 2008). For example, most models assume that the specific angular momentum of galaxies and halos are similar, and that the merger history of the halos dictates that of the central galaxy.

Recent developments, however, have led to revisiting some of the assumptions of the simple scenario outlined above. For example, it has become clear that major mergers are rare, and therefore probably not the primary formation mechanism of bulges and ellipticals. Instead, “disk instabilities” (Efstathiou et al. 1982; Christodoulou et al. 1995; Mo et al. 1998), as well as repeated minor encounters, are now claimed to be the main formation path of spheroids (e.g., Parry et al. 2009; Hopkins et al. 2010; De Lucia et al. 2011; Bournaud et al. 2011). This has helped to alleviate some tension between the observed evolution of the early-type galaxy population and the major-merger rates predicted by theory (Bundy et al. 2007; Oesch et al. 2010).

Further scrutiny has come from direct simulation of hierarchical galaxy formation. Conserving enough angular momentum during the hierarchical assembly of a galaxy to form a realistic stellar disk has been challenging (see, e.g., Navarro et al. 1995; Navarro & Steinmetz 1997), as has been pinning down the effect on morphology of repeated merging, especially between gas-rich galaxies (see, e.g., Robertson et al. 2006; Governato et al. 2009).

The inclusion of energetic feedback, needed to prevent the formation of too many faint or overly massive galaxies, has added an extra level of complexity to the problem, with a number of studies showing that morphologies can be radically altered when even modest changes in the strength of feedback or its implementation are introduced (Okamoto et al. 2005; Scannapieco et al. 2008; Ceverino & Klypin 2009; Sales et al. 2010; Agertz et al. 2011; Piontek & Steinmetz 2011). These differences in morphologies are often traced back to variations of the final spin content of galaxies caused by a delayed condensation of baryons into sub-galactic clumps (Zavala et al. 2008) and the preferential removal of material with low angular momentum (Brook et al. 2011).

More recently, the *mode* of gas accretion has been recognized as playing a potentially crucial role in galaxy morphology. Gas can flow to galaxies largely unimpeded by shocks (White & Frenk 1991) and may be collimated by the filamentary structure of the cosmic web, especially in low-mass systems

and at high redshift (Kereš et al. 2005; Dekel & Birnboim 2006; van de Voort et al. 2011). This complex accretion geometry has been hypothesized to promote the formation of disks by feeding high angular momentum material directly to forming galaxies (see, e.g., Dekel et al. 2009; Brooks et al. 2009).

Further theoretical progress demands increased sophistication in numerical and semi-analytic modeling. From the simulation perspective, most studies have focussed on individual systems picked according to what the authors believe would facilitate the formation of a galaxy of predetermined morphology; for example, a recent major merger to study ellipticals (e.g., Meza et al. 2003) or a quiet, rapidly-rotating halo to study spirals (e.g., Abadi et al. 2003; Governato et al. 2007). Note that this presupposes the morphology of the resulting galaxy, and often results in the tuning of star formation and feedback parameters until, unhelpfully, results match prejudice.

Statistically-significant samples of galaxies selected in an unbiased way and simulated at high resolution are needed for new insights, a goal that, despite valiant efforts (Croft et al. 2009; Sales et al. 2009, 2010), has so far proved beyond reach of even the fastest computers and best algorithms. The situation, however, is starting to change, with the advent of simulations of volumes large enough to include dozens of well-resolved  $\sim L_*$  galaxies (Crain et al. 2009; Schaye et al. 2010; Hahn et al. 2010; Cen & Chisari 2011; Vogelsberger et al. 2011).

We explore these issues here using the GIMIC gasdynamical simulation series (Crain et al. 2009). GIMIC targeted several carefully selected regions from the Millennium Simulation (Springel et al. 2005) in an attempt to maximize the resolution of individual galaxy systems while at the same time sampling a cosmologically-significant volume. The first analyses of  $z = 0$  GIMIC galaxies (Crain et al. 2010; Font et al. 2011; McCarthy et al. 2011) show that they are fairly realistic, so we feel confident that we can use them to gain insight into the origin of galaxy morphology.

This paper is organized as follows. In Sec. 2 we present briefly the numerical method and simulations. We analyze the morphologies of simulated galaxies and their origin in Secs. 3 and 4, respectively. We summarize our main conclusions in Sec. 5

## 2 NUMERICAL SIMULATIONS

The “Galaxies-Intergalactic Medium Interaction Calculation”, (GIMIC; Crain et al. 2009), simulation series follows the evolution of five nearly spherical regions of radius  $\sim 20 h^{-1}$  Mpc each, selected from the *Millennium Simulation* (Springel et al. 2005). These regions were selected to sample environments of different density, deviating by  $(-2, -1, 0, +1, +2)\sigma$  from the cosmic average, respectively, where  $\sigma$  is the *rms* mass fluctuation on  $20 h^{-1}$  Mpc scales. The regions are spherical at  $z = 1.5$ , and are simulated using the standard zoom-in technique described in detail by, e.g., Power et al. (2003). We provide here a basic summary of the main characteristics of the GIMIC project, and refer the interested reader to Crain et al. (2009) for a more comprehensive description.

GIMIC uses a modified version of GADGET-3, a development of the GADGET-2 code (Springel 2005) that includes new modules to treat radiative cooling, star formation, chemical enrichment, and energetic feedback. Radiative cooling is implemented on an element-by-element basis and thus cooling rates evolve self-consistently as a function of redshift, gas density, temperature and

chemical composition (Wiersma et al. 2009). The runs also include a uniform ionizing background (Haardt & Madau 2001), with hydrogen- and helium-reionization redshifts of  $z = 9$  and  $z = 3.5$ , respectively.

Cold gas with densities exceeding  $n_H = 0.1 \text{ cm}^{-3}$  becomes eligible for star formation and is assumed to follow an effective equation of state,  $P \propto \rho^{4/3}$ , in order to minimize numerical artifacts in poorly-resolved regions (Schaye & Dalla Vecchia 2008). Stars are assumed to follow a Chabrier IMF (Chabrier 2003), and to form at a rate that depends on the local gas pressure and that matches the Kennicutt-Schmidt law (Kennicutt 1989, 1998).

Chemical enrichment is modeled as described by Wiersma et al. (2009), and tracks the synthesis of 11 individual elements. As massive stars explode as supernova (SN), they inject energy and metals into their surroundings. This feedback is implemented, in practice, by using a fraction  $f_{SN}$  of the energy released by SN in order to modify the velocity of a few ( $\eta_w$ ) neighboring gas particles by introducing a velocity “kick” of magnitude  $V_w$  to each (Dalla Vecchia & Schaye 2008). These parameters are set in GIMIC to  $f_{SN} = 0.8$ ,  $\eta_w = 4$  and  $V_w = 600 \text{ km/s}$ , which results in a good match to the peak of the global star formation rate density (Crain et al. 2009; Schaye et al. 2010).

All GIMIC runs adopt the same cosmological parameters as the original *Millennium Simulation*, which were chosen to be consistent with the WMAP-1 constraints:  $\Omega_m = 0.25$ ;  $\Omega_\Lambda = 0.75$ ;  $\Omega_b = 0.045$ ;  $n_s = 1$ ;  $H_0 = 100 h \text{ km s}^{-1} \text{ Mpc}^{-1}$ ;  $h = 0.73$ .

The particle mass in the simulations is  $1.4 \times 10^6 h^{-1} M_\odot$  and  $6.6 \times 10^6 h^{-1} M_\odot$  for the baryons and dark matter, respectively. The gravitational softening is initially fixed in comoving units, but is fixed at  $z = 3$  and thereafter to  $\epsilon = 0.5 h^{-1} \text{ kpc}$  (Plummer equivalent) in physical units. We shall focus here on the two GIMIC regions that have been run to  $z = 0$  at this resolution: the  $-2\sigma$  and  $0\sigma$ . As we discuss below, aside from the expected difference in the number of systems of given mass, we see no systematic dependence of our results on the overdensity of the region, which may therefore be thought to apply to average regions of the Universe.

We have used SUBFIND (Springel et al. 2001; Dolag et al. 2009) to identify galaxies in the high-resolution regions of the GIMIC runs. We shall only consider in the analysis the *central* galaxies of halos within a narrow range of virial<sup>1</sup> mass:  $0.5 < M_{200}/10^{12} h^{-1} M_\odot < 1.5$ . This ensures homogeneity in the set of systems selected for analysis and eliminates complications that may arise from considering satellites of larger systems. At redshift  $z = 0$ , these criteria identify 38 and 62 galaxies in the  $-2\sigma$  and  $0\sigma$  runs, respectively. Each of these halos is resolved with roughly 200,000 particles (dark plus baryonic), allowing for a reasonable estimate of the relative importance of the disk and spheroidal components. None of the results we discuss here show significant dependence on which region we consider, so we will group the 100 galaxies together without making any distinction regarding the GIMIC run where they were identified.

<sup>1</sup> Virial quantities throughout this paper are defined at the radius enclosing 200 times the critical density for closure.

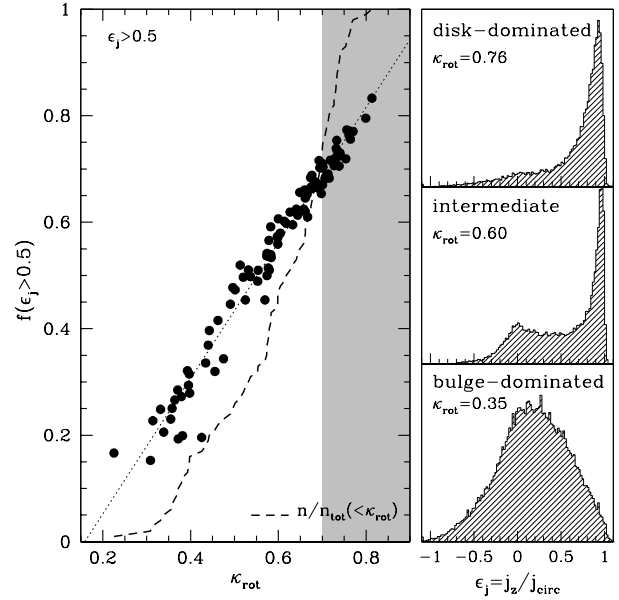


**Figure 1.** *Left:* The kinematic morphology parameter,  $\kappa_{\text{rot}}$ , defined as the fraction of kinetic energy in organized rotation (eq. 1), versus the fraction of stars with circularity parameter  $\epsilon_j > 0.5$ . The cumulative fraction is shown with a dashed line. The shaded region ( $\kappa_{\text{rot}} > 0.7$ ) indicates where “disk dominated” galaxies lie in this plot. *Right:* The distribution of circularities,  $\epsilon_j = j_z / j_{\text{circ}}(E)$ , is shown for three galaxies with different values of  $\kappa_{\text{rot}}$ .

**Table 1.** Summary of main properties for Gal A-D in Fig. 2 and 3. Rows correspond to the virial mass  $M_{200}$ ; galactic mass in stars  $M_{\text{str}}$ ; gas  $M_{\text{gas}}$  and gas fraction  $f_{\text{gas}}$ ; peak circular velocity  $V_{\text{max}}$ ; the circular velocity measured at the galactic radius  $V_c(r = r_{\text{gal}})$ ; the degree of rotational support  $\kappa_{\text{rot}}$ ; and the fraction of the stars in counter-rotating orbits  $f_c$ .

Property	Gal A	Gal B	Gal C	Gal D
$M_{200} [10^{12} h^{-1} M_\odot]$	1.18	0.98	0.77	1.04
$M_{\text{str}}(r < r_{\text{gal}}) [10^{10} h^{-1} M_\odot]$	8.98	7.25	5.42	6.31
$M_{\text{gas}}(r < r_{\text{gal}}) [10^{10} h^{-1} M_\odot]$	0.51	0.72	1.00	1.86
$f_{\text{gas}}(M_{\text{gas}} / (M_{\text{gas}} + M_{\text{str}}))$	0.05	0.09	0.15	0.23
$V_{\text{max}}$ [km/s]	471	383	300	280
$V_c(r = r_{\text{gal}})$ [km/s]	187	172	160	178
$\kappa_{\text{rot}}$	0.31	0.47	0.61	0.76
$f_c$	0.48	0.33	0.12	0.06

### 3 SIMULATED GALAXY MORPHOLOGIES

#### 3.1 Morphology estimates

As discussed in Sec. 1, we shall adopt a somewhat narrow definition of morphology based on the importance of ordered rotation in the structure of a galaxy. Although we refer to this as the ratio of disk to spheroid, it should be noted that this may differ, at times substantially, from traditional bulge-to-disk decompositions based on photometric data. The latter are based on assumptions regarding the shape of the brightness profile of disks, usually assumed to be exponential, and spheroids, assumed to follow either de Vaucouleurs or Sersic profiles. As discussed by Abadi et al. (2003) (see

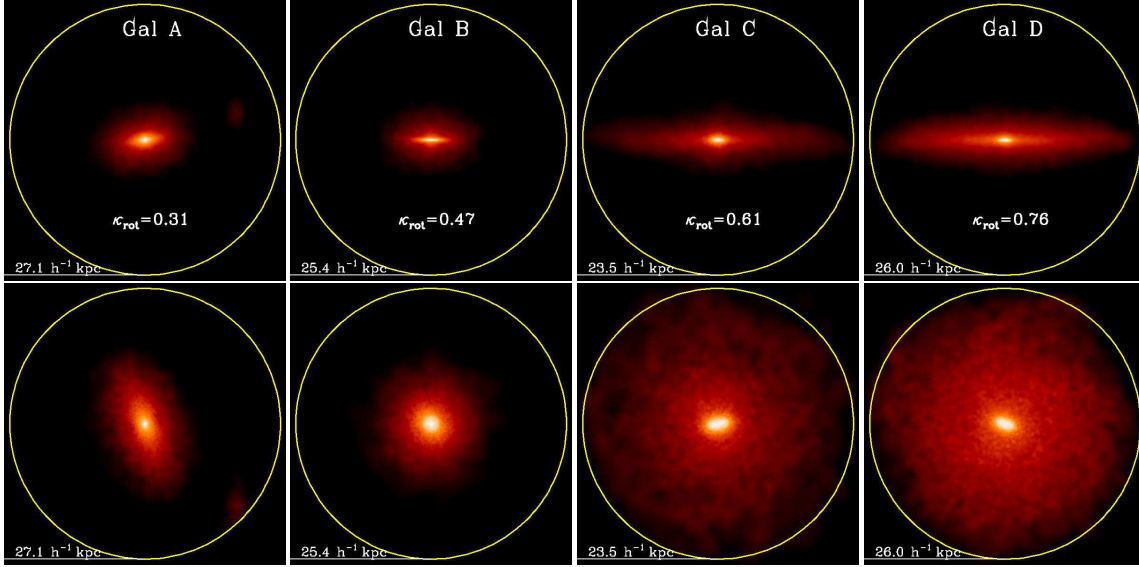


**Figure 2.** Illustration of the structure of four galaxies in our sample with increasing degree of rotational support (left to right). The first and second rows show edge-on and face-on projections of the stellar distribution. The yellow circle marks the radius,  $r_{\text{gal}} = 0.15 r_{200}$ , used to define the galaxy.

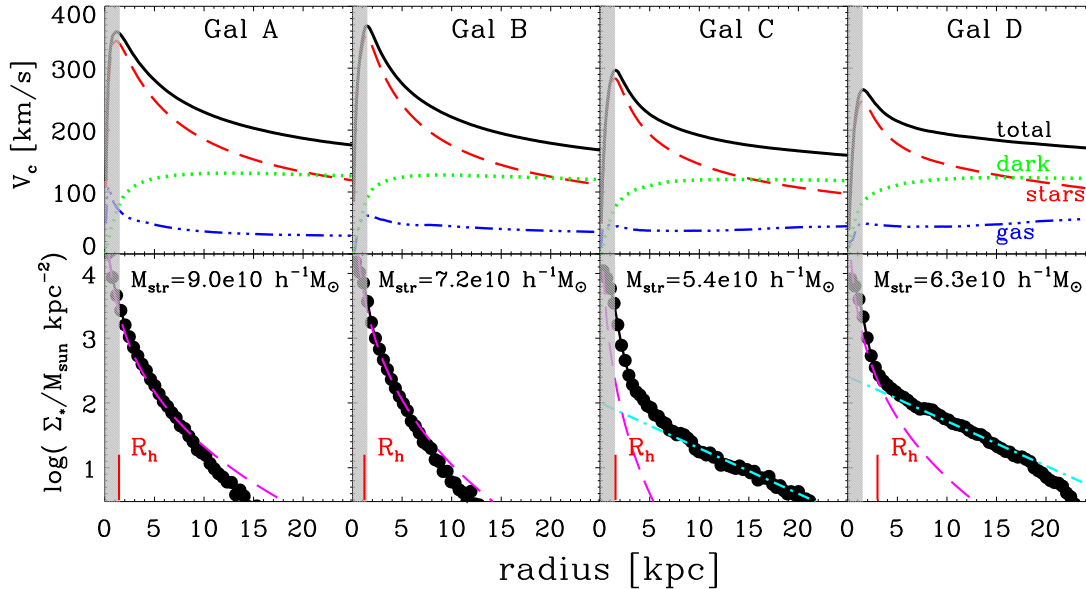


**Figure 3.** Top and bottom rows show the circular velocity profile,  $V_c(r)$ , and the stellar surface density profiles, respectively, of galaxies A-D in Fig. 2. Red lines in the bottom panels indicate the stellar half-mass radius of each galaxy. Dashed magenta lines indicate de Vaucouleurs'  $R^{1/4}$  profile fits. Straight dashed lines in blue indicate exponential profile fits. The shaded area highlights a radius equal to three Plummer-equivalent gravitational softening scalelengths. Note that spheroids can be well fit by a single  $R^{1/4}$  law, but that disk-dominated galaxies show evidence of a de Vaucouleurs' spheroid plus an exponential disk. Disks are extended and have approximately flat circular velocity curves, spheroids tend to be denser and to have declining  $V_c$  curves.

also Scannapieco et al. 2010), these assumptions are only weakly fulfilled by simulated galaxies, and kinematic decompositions can give rather different spheroid-to-disk ratios than photometric ones. Photometric studies can also be affected by color gradients, extinction, and projection effects (see, e.g., Governato et al. 2009). We avoid these complications by focusing our analysis on kinematic data alone, although we plan to consider the implications of our results for photometric studies in future work.

The importance of ordered rotation may be clearly appreciated from the distribution of the stellar orbital circularity parameter,  $\epsilon_j = j_z/j_{\text{circ}}(E)$ , defined as the ratio of the specific angular

momentum perpendicular to the disk to that of a circular orbit with the same binding energy,  $E$ . Defined in this way,  $\epsilon_j$  takes values in the range  $(-1,1)$ , corresponding to the counter- and co-rotating circular orbits, respectively.

We show the  $\epsilon_j$  distribution in the right-hand panels of Fig. 1 for three simulated galaxies, chosen to illustrate three representative cases. The top panel corresponds to a galaxy where most stars are in coplanar, nearly circular orbits, hence the sharply-peaked distribution near  $\epsilon_j = 1$ . The bottom panel corresponds to a spheroidal galaxy where ordered rotation plays little role; the  $\epsilon_j$  distribution is broad and centered around zero. The middle panel corresponds to

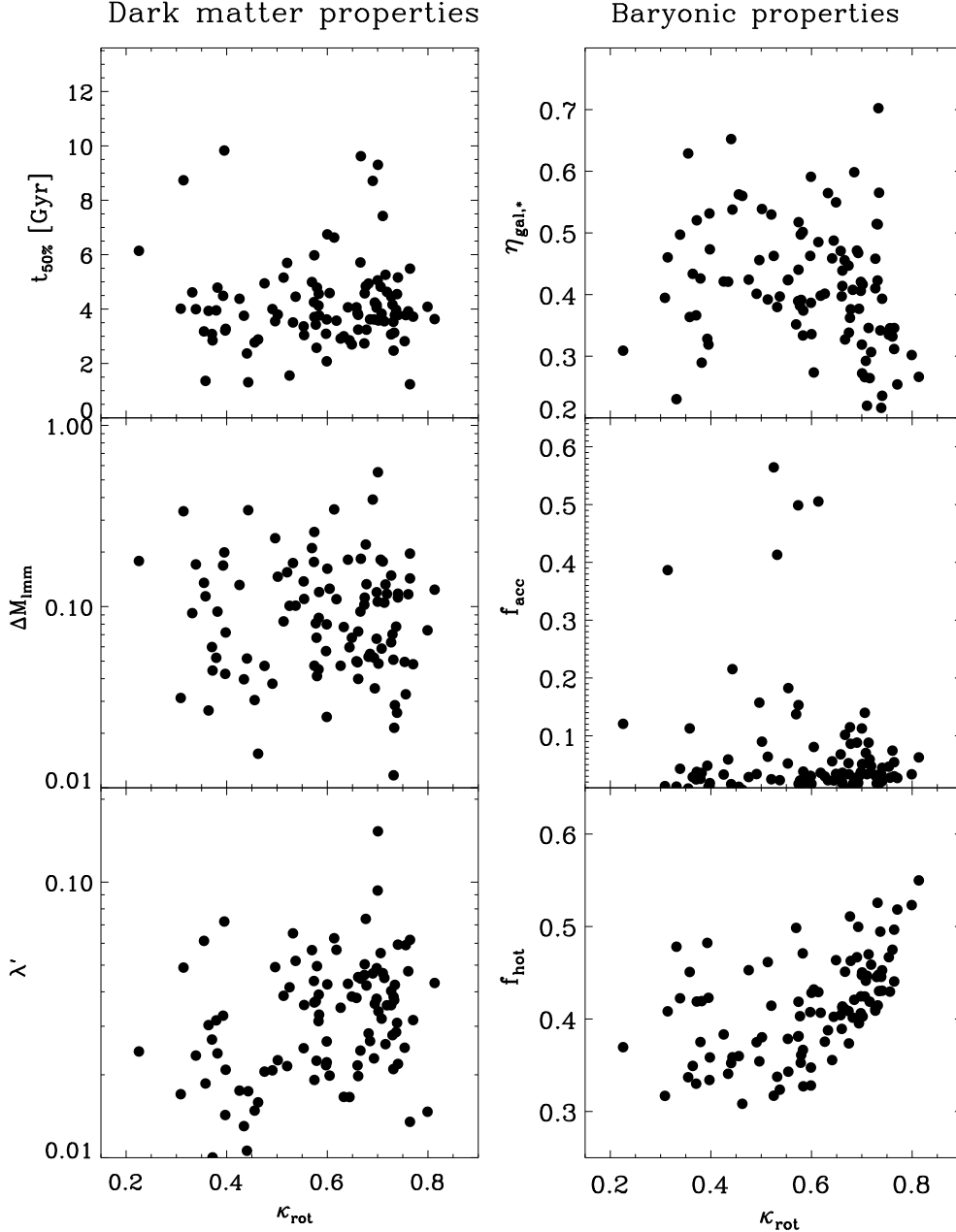


**Figure 4.** The kinematic morphology parameter,  $\kappa_{\text{rot}}$ , versus a number of parameters characterizing the properties and assembly history of each galaxy and its surrounding halo. On the left, from top to bottom,  $t_{50\%}$  is the half-mass halo formation time, in Gyrs;  $\Delta M_{\text{imm}}$  is the maximum fraction of the final halo mass assembled in the single largest merger event after  $z = 3$ ; and  $\lambda'$  is the dimensionless rotation parameter (eq. 2). On the right, the galaxy formation “efficiency”,  $\eta_{\text{gal},*} = M_{\text{gal},*}/(f_{\text{bar}}M_{200})$ ;  $f_{\text{acc}}$  is the fraction of *accreted* stars (i.e., stars formed in galaxy progenitors other than the main one) and  $f_{\text{hot}}$  is the fraction of stars born out of gas that went through the “hot phase” (i.e.,  $T > 10^{5.5}$  K). Correlation coefficients for each panel are given in Table 2. See text for further details.

an intermediate case, where a non-rotating bulge of stars is surrounded by a well-defined thin disk. A simple quantitative measure of morphology can therefore be constructed by the fraction of stars with circularities exceeding a fixed fiducial value, such as  $f(\epsilon_j > 0.5)$ .

Although conceptually simple,  $\epsilon_j$  distributions are not easy to measure observationally, so a simpler quantitative measure of morphology would be desirable. One alternative is the fraction of kinetic energy invested in ordered rotation,

$$\kappa_{\text{rot}} = \frac{K_{\text{rot}}}{K} = \frac{1}{K} \sum \frac{1}{2} m \left( \frac{j_z}{R} \right)^2. \quad (1)$$

$\kappa_{\text{rot}} \sim 1$  for disks with perfect circular motions, and is  $\ll 1$  for

**Table 2.** Spearman rank correlation coefficients,  $r_s$ , between  $\kappa_{\text{rot}}$  and the halo/galaxy properties shown in Figs. 4 and 8. The second column shows the two-sided significance of its deviation from zero, as computed by the IDL subroutine `r-correlate`: smaller values indicate more significant correlations.

Property	$r_s$	$\Delta$
$t_{50\%}$	0.05	0.60
$\Delta_{1\text{mm}}$	-0.06	0.57
$\lambda'$	0.29	$2.8 \times 10^{-3}$
$\eta_{\text{gal},*}$	-0.30	$1.9 \times 10^{-3}$
$f_{\text{acc}}$	0.06	0.55
$f_{\text{hot}}$	0.55	$1.6 \times 10^{-9}$
$\langle \cos(\theta) \rangle$	0.41	$2.0 \times 10^{-5}$

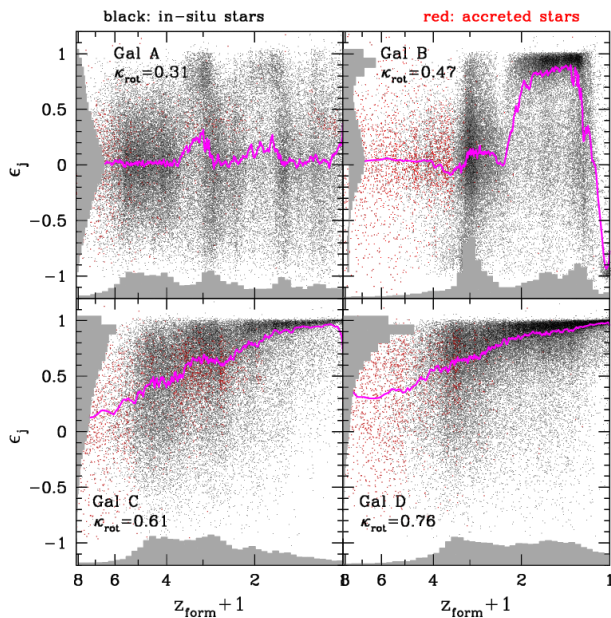


**Figure 5.** Formation time of stars (expressed in terms of redshift) versus the circularity parameter,  $\epsilon_j$ , measured at  $z = 0$ , for the four galaxies illustrated in Fig. 2. Stars formed in the main progenitor (in situ) are shown in black, accreted stars in red. The magenta curve tracks the median circularity as a function of formation time. The two spheroid-dominated galaxies show signs of episodic star formation events that lead to the presence, at  $z = 0$ , of stellar populations with distinct angular momentum properties. Disks, on the other hand, tend to form more gradually over time and to be dominated by a single population with coherently-aligned angular momentum.

non-rotating systems. As Fig. 1 makes clear,  $\kappa_{\text{rot}}$  correlates extremely well with the fraction of stars with  $\epsilon > 0.5$ . In what follows, we shall use  $\kappa_{\text{rot}}$  to rank galaxies according to the importance of their rotationally-supported components.

For convenience, we shall hereafter refer to galaxies with  $\kappa_{\text{rot}} < 0.5$  and  $\kappa_{\text{rot}} > 0.7$  as spheroid- or disk-dominated, respectively. The first group makes up  $\sim 25\%$  of the sample; the second group comprises another  $\sim 30\%$ . The remainder consist of intermediate types where both rotation and velocity dispersion play a comparable structural role. It is important to note that all values of  $\kappa_{\text{rot}}$  are well represented in our sample, from pure “bulgeless” disks to spheroids with little trace of rotational support.

### 3.2 Examples of galaxy morphologies

Fig. 2 shows four examples chosen to illustrate the structure of galaxies with various values of  $\kappa_{\text{rot}}$ . The panels show edge-on and face-on projections of each galaxy, colored by stellar surface mass density on a logarithmic scale. Fig. 3 shows circular velocity profiles and (face-on) stellar surface density profiles. The degree of rotational support increases from left to right: the leftmost and rightmost are spheroid- and disk-dominated systems, respectively, while the two middle ones are intermediate-type objects. Labels in each panel indicate, for each galaxy, the stellar mass within the radius,  $r_{\text{gal}} = 0.15 r_{200}$ , used to define the central galaxy. Table 1 lists some physical parameters of galaxies A-D.

Figs. 2 and 3, together with Table 1, show that simulated galaxies have several properties in common with nearby ellipticals and spirals. Spheroid-dominated galaxies are gas-poor, dense stellar systems with declining circular velocity curves, whereas disk-dominated galaxies are richer in gas, more spatially extended, and have nearly-flat circular velocity curves. Interestingly, from the point of view of surface density profiles, spheroids are single-component systems well approximated by de Vaucouleurs’  $R^{1/4}$  law (dashed magenta lines in the bottom panels of Fig. 3). Disk-dominated systems, on the other hand, have more complex profiles, with a central  $R^{1/4}$  spheroid surrounded by an exponential component that increases in importance in step with  $\kappa_{\text{rot}}$ . Like most spirals, they are well approximated by the sum of a de Vaucouleurs’ spheroid (dashed magenta lines) and an exponential law (dashed cyan lines).

As discussed in detail by McCarthy et al (in preparation), these similarities with observation actually extend to quantitative comparisons with observed scaling laws, such as the Tully-Fisher relation or the Fundamental Plane. The agreement between simulated galaxies and observation is encouraging, and suggests that the origin of the morphological diversity of simulated galaxies may provide insight into what determines the relative importance of disks and spheroids in real galaxies.

## 4 THE ORIGIN OF SIMULATED GALAXY MORPHOLOGIES

### 4.1 Halo dependence

As discussed in Sec. 1, stellar disks are expected to form at the centers of halos with quiet recent accretion histories and high angular momentum. Halos that have been relatively undisturbed by recent major mergers tend to form earlier, so we may also expect stellar disks to inhabit halos with early formation times.

We explore these ideas in Fig. 4, where the left panels show the dependence of  $\kappa_{\text{rot}}$  on (i) the halo formation time,  $t_{50\%}$  (when the most massive halo progenitor reaches half the final halo mass); on (ii) the fraction of halo mass accreted in the single largest merger after  $z = 3$ ,  $\Delta M_{1\text{mm}}$ , and on (iii) the dimensionless rotation parameter,

$$\lambda' = \frac{1}{\sqrt{2}} \frac{J}{M_{200} V_{200} r_{200}}, \quad (2)$$

where  $J$  is the total angular momentum of the halo (Bullock et al. 2001).

None of these parameters correlates strongly with galaxy morphology (see Table 2). Disks form in halos with low and high spin parameter; in halos that collapse early and late, and even in halos

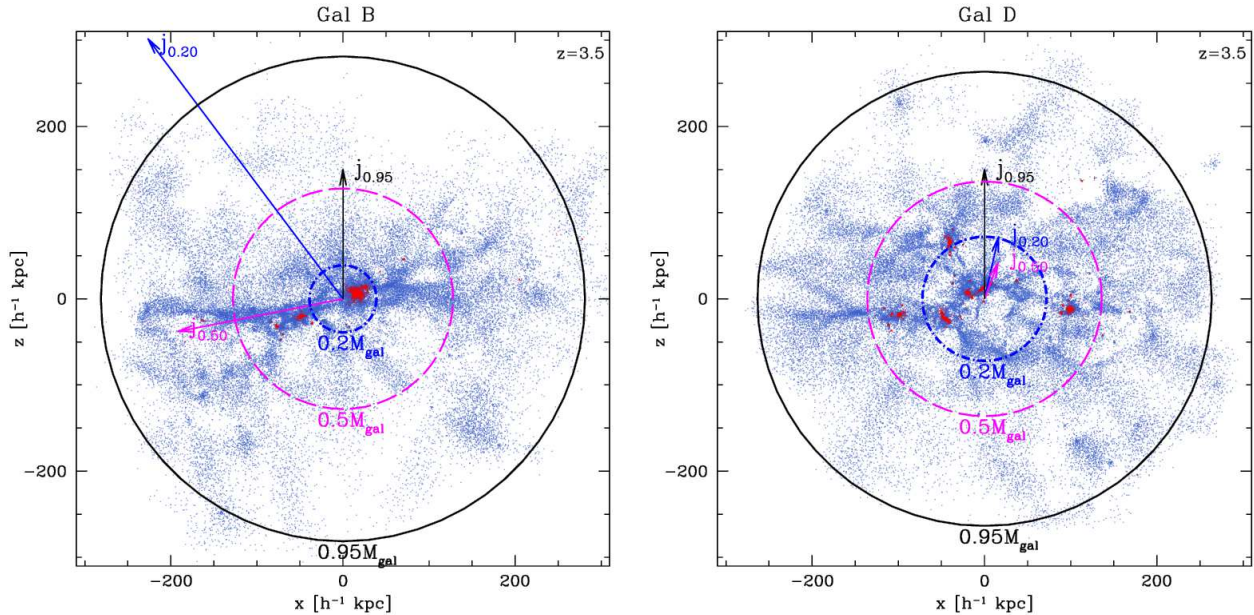


**Figure 6.** Projected particle distribution near turnaround time,  $z = 3.5$ , of baryons that collapse to form, at  $z = 0$ , galaxies B and D shown in Fig. 2. Stars already formed are shown in red, particles still in gaseous form in blue. Box sizes are in physical units. Concentric circles enclose 25%, 50%, and 95% of the mass, and arrows indicate the angular momentum of all material enclosed within each radius. Arrow lengths are normalized to the total value, which defines the  $z$  axis of the projection. Each panel is normalized separately, so that  $j_{0.95}$  has equal length in both. Note the misalignment of the angular momentum of various parts of the system for the spheroid-dominated galaxy B. Angular momentum is more coherently acquired in the case of the disk-dominated galaxy D.

that have accreted a substantial amount of mass in merger events. The same applies to spheroids, except perhaps for a weak tendency to prefer halos with slightly lower-than-average  $\lambda'$ .

Fig. 4 also shows that major mergers are uncommon during the formation of halos in the narrow mass range considered here;  $0.5 < M_{200}/10^{12} h^{-1} M_{\odot} < 1.5$ . Most systems have accreted less than 20% of their final mass in a single merger since  $z = 3$ , and these events seem unrelated to the morphology of the central galaxy at  $z = 0$ .

Finally, morphology also seems unrelated to the fraction of baryons within the virial radius that collects to form the galaxy. This is illustrated in the top-right panel of Fig. 4, where we plot  $\kappa_{\text{rot}}$  vs the galaxy formation “efficiency” parameter,  $\eta_{\text{gal},*} = M_{\text{gal},*}/(f_{\text{bar}} M_{200})$ , where  $f_{\text{bar}} = \Omega_b/\Omega_m = 0.175$  is the universal baryon fraction. Although we consider halos in a narrow mass range, the efficiency of galaxy formation varies from 20% to 70% (with an average of  $\langle \eta_{\text{gal},*} \rangle = 40\%$ ) and appears to have little influence on the morphology of the central galaxy, although there is a weak tendency for disk-like objects to prefer lower values of  $\eta_{\text{gal},*}$ .

Thus, contrary to simple expectations, spheroids *can* form in quiescent halos, and disks *can* form in halos of scant angular momentum content. Simple predictions of the morphology of a galaxy based on the properties and assembly history of its surrounding dark halo will thus often be wrong.

## 4.2 Dependence on galaxy history

Galaxy mergers can still in principle play a role in determining morphology, if their importance is underestimated by the *halo* merger parameter  $\Delta M_{\text{1mm}}$ . Indeed, galaxies take longer to merge than ha-

los do, and, due to the large scatter in galaxy formation efficiency, the mass ratio of galaxy mergers may differ substantially from that of their surrounding halos.

We examine the importance of accretion on morphology more explicitly in the middle-right panel of Fig. 4, where we plot  $\kappa_{\text{rot}}$  vs  $f_{\text{acc}}$ , the fraction of stars *accreted* by the galaxy; i.e., those formed in systems *other* than the main progenitor of the galaxy. This is a direct measure of the importance of accretion events in the build-up of the galaxy. Two points are worth noting here: most galaxies form the majority ( $> 90\%$ ) of their stars *in-situ*, and there is no correlation between  $\kappa_{\text{rot}}$  and  $f_{\text{acc}}$ . The accreted fraction exceeds 25% in only 5 of our 100 simulated galaxies; overall, accretion events just seem to bring in too few stars to play a significant role in the morphology of our simulated galaxies.

An interesting clue is provided by the thermodynamic history of the gas before it is transformed into stars. This may be estimated simply by tracking every stellar particle back in time and by recording the maximum temperature,  $T_{\text{max}}$ , reached before the particle accretes into the galaxy and becomes eligible for star formation. If  $T_{\text{max}}$  exceeds  $10^{5.5}$  K, then in all likelihood it was accreted by gradual cooling from a shock-heated, nearly hydrostatic corona of gas (see, e.g., Crain et al. 2010; van de Voort et al. 2011).

The fraction of stars,  $f_{\text{hot}}$ , whose parent gas particles went through this phase correlates well with  $\kappa_{\text{rot}}$ , indicating that accretion of gas from the “hot phase” favours the formation of disks (see bottom-right panel of Fig. 4). No disk-dominated galaxy (i.e.  $\kappa_{\text{rot}} > 0.7$ ) forms unless  $f_{\text{hot}}$  exceeds 40%. This is intriguing, since it runs counter recent proposals that “cold flows”, i.e., gas that gets accreted directly into the galaxy without going through the hot phase, might promote the formation of extended disks (e.g., Kereš et al. 2005; Dekel et al. 2009; Brooks et al. 2009). If anything, our simulations suggest the opposite; the majority of stars in

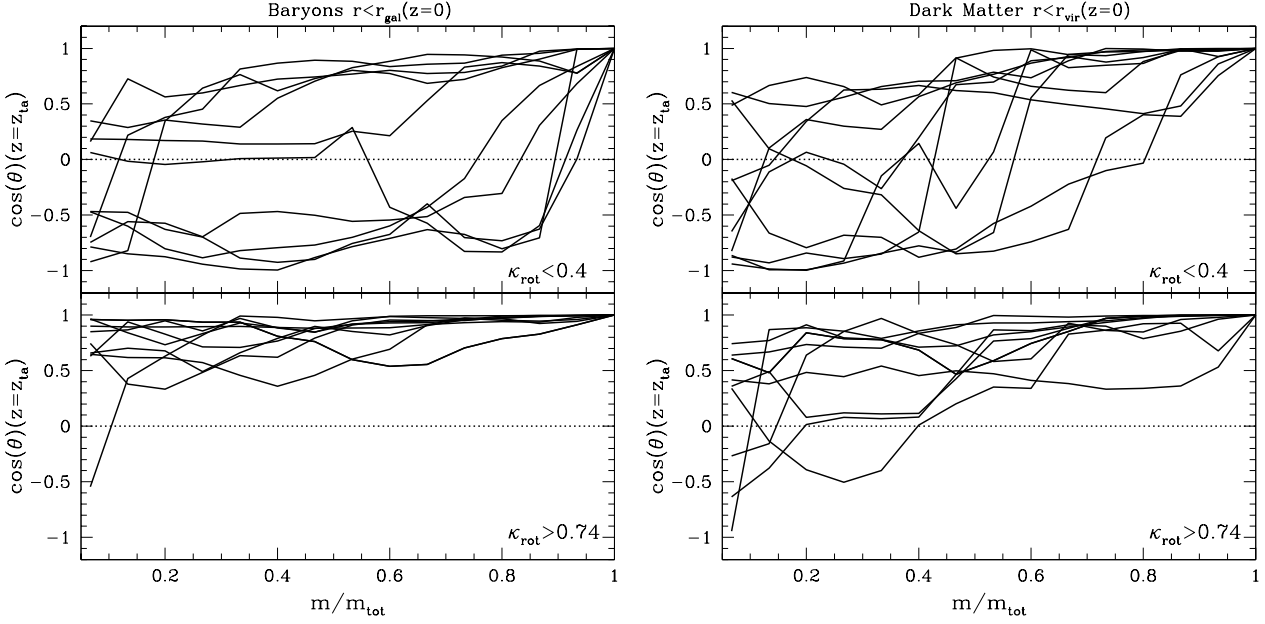


**Figure 7.** Angle between the angular momentum enclosed within a given mass fraction,  $m/m_{\text{tot}}$ , and the total spin of the system measured at the time of maximum expansion (turnaround) for twenty galaxies in our sample: the ten systems with highest and lowest values of  $\kappa_{\text{rot}}$  at  $z = 0$  and  $f_{\text{acc}} < 0.1$ , respectively. The restriction in  $f_{\text{acc}}$  is included in order to focus on systems unaffected by merger events. By definition, all curves approach unity as  $m \rightarrow m_{\text{tot}}$ . Panels on the left correspond to all baryons within the galaxy radius,  $r_{\text{gal}}$ , at  $z = 0$ ; those on the right to dark matter halo particles that are within  $r_{200}$  at  $z = 0$ . Note the strong misalignments between different parts of the system for galaxies that are spheroid-dominated at  $z = 0$ , and the smooth alignment characteristic of the turnaround configuration of systems destined to become disks.

spheroid-dominated galaxies originate in gas that accretes through such “cold flows”.

### 4.3 Dependence on spin alignment

Our results so far suggest that the morphology of GIMIC galaxies is linked to internal mechanisms operating in individual galaxies rather than to accretion-driven transformations. This has been anticipated by semi-analytic models of galaxy formation, where secular evolution driven by “disk instabilities”, is thought to be an important formation path for spheroids. These instabilities are assumed to be triggered when the self-gravity of a disk exceeds a particular threshold. For fixed halo mass, as in our sample, this should lead to noticeable correlations between the mass of the galaxy and the importance of the spheroid. However, as we discussed above, no such correlation is apparent.

Recalling the correlation between  $f_{\text{hot}}$  and  $\kappa_{\text{rot}}$ , we look at the formation redshift,  $z_{\text{form}}$ , of stars in the four galaxies shown in Fig. 2 versus the “circularity” parameter,  $\epsilon_j$ , measured at  $z = 0$ . Points in black correspond to stars formed *in-situ* (i.e., within the main progenitor) while those in red are accreted stars.

This figure shows that, as expected, star formation proceeds gradually in disk-dominated systems. In spheroids, however, stars form in separate episodes that leave behind stellar “populations” of different ages and distinct angular momenta. Since most stars form *in-situ*, these populations in galaxies A and B are likely caused by gas accretion events where the net angular momentum of one event is misaligned with the others.

On the other hand, disks tend to form out of accreted gas that

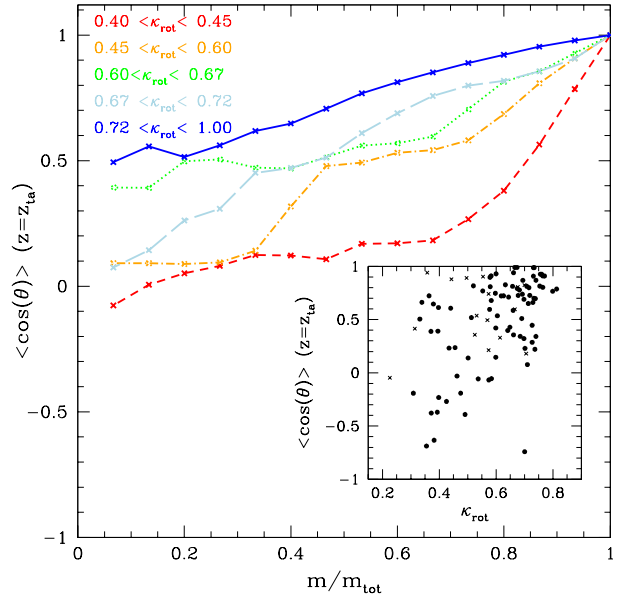


**Figure 8.** Same as left-hand panel of Fig. 7, but averaged over all galaxies grouped in bins of  $\kappa_{\text{rot}}$  (at  $z = 0$ ), as labeled. Note that the more disk-dominated a galaxy is at present, the more coherently aligned the spin is at the time of turnaround. The inset panel shows  $\langle \cos(\theta) \rangle$  for individual systems, averaged over all mass shells at turnaround, as a function of  $\kappa_{\text{rot}}$ . Galaxies where accretion events have played a minor role, i.e.,  $f_{\text{acc}} < 0.1$ , are shown with solid circles, the rest with crosses.

shares a common angular momentum direction. This explains why accretion from a hot gaseous corona favours disk formation: gas shock-heated into a nearly-hydrostatic corona of hot gas is forced to homogenize its rotational properties before accretion, providing the forming galaxy with gas that shares the same spin axis.

It also suggests an explanation for why gas that gets accreted “cold” tends to favour spheroid formation: gas that flows along distinct filaments cannot interact hydrodynamically before accretion and will therefore often have misaligned net spins. Each accretion event then results in the formation of a “population” of misaligned stars that will tend to destabilize any existing disk and to cancel out the net angular momentum of the system, leaving in place a slowly-rotating stellar spheroid.

In other words, spheroids do not originate from disk instabilities triggered by the disk self-gravity, as envisioned by semi-analytic models, but rather by the accretion of gas that settles on off-axis orbits relative to earlier accreted material. This has been seen in earlier work (e.g., Brook et al. 2008; Scannapieco et al. 2009), and might be related to sudden changes in the orientation of the dark matter halos as discussed in Bett & Frenk (2011), but its relevance to the formation of the whole class of spheroidal galaxies has not yet been recognized and emphasized.

These considerations suggest that the final morphology of a galaxy is imprinted early on, since the angular momentum of the material destined to form a galaxy is acquired at the time of maximum expansion and changes little in the absence of merging (see, e.g., White 1984; Navarro et al. 2004). We illustrate this by studying the angular momentum of galaxies B and D at  $z = 3.5$ , which roughly corresponds to the time of turnaround of both systems. Fig. 6 shows the spatial distribution of all baryons that will end up within  $r_{\text{gal}}$  at  $z = 0$ . Net angular momentum is acquired through the interplay between the inertia tensor of the mass distribution and the shear tensor due to the large-scale distribution of surrounding matter, so that the direction of the acquired spin usually aligns with the *intermediate axis* of the mass distribution (Catelan & Theuns 1996; Porciani et al. 2002a,b; Navarro et al. 2004). For highly non-uniform spatial distributions, where the principal axes of the inertia tensor can change direction abruptly, this effect may cause the net angular momentum of different parts of the system to flip and misalign.

We see from Fig. 6 that this is indeed the case for galaxy B. Here the arrows indicate the direction and magnitude, at  $z = 3.5$ , of the specific angular momentum of the inner 20%, 50% and 95% of the baryons that end up in the galaxy at  $z = 0$ . The length of the arrows is normalized to the total, which is chosen by construction to coincide with the  $z$  axis of the projection. The angular momenta of different parts of the system are clearly misaligned: the angle between  $\mathbf{j}_{0.2}$  and  $\mathbf{j}_{0.5}$  is 85 degrees, and that between  $\mathbf{j}_{0.5}$  and  $\mathbf{j}_{0.95}$  is  $\sim 100$  degrees. Since gas further out in Fig. 6 takes longer to accrete, if the galaxy grows through direct “cold” accretion of gas, in general newly accreted material will be misaligned with the rest, leading to the formation of the distinct populations of stars shown in Fig. 5.

On the other hand, the spins of different parts of the system are very well aligned in the case of the disk-dominated galaxy D, as shown in Fig. 6. This coherence in the angular momentum at turnaround allows newly accreted material to settle into a stable disk where star formation can proceed gradually and smoothly.

We show in Fig. 7 that this result applies to the majority of spheroid- and disk-dominated galaxies in our sample. Here we plot, for the ten galaxies with highest and lowest values of  $\kappa_{\text{rot}}$  where accretion has played a minor role ( $f_{\text{acc}} < 0.1$ ), the cosine of the

angle  $\theta$  between the angular momentum of a given enclosed mass fraction  $m/m_{\text{tot}}$  and the direction of the total spin of the system. By construction, each curve in Fig. 7 is constrained to approach unity as the enclosed mass approaches  $m_{\text{tot}}$ .

It is clear from this figure that different regions of systems destined to form spheroid-dominated galaxies have, at turnaround, large misalignments in their acquired spin. Indeed, in many cases the inner regions counterrotate (i.e.,  $\cos(\theta) < 0$ ) relative to the outer regions of the system. This is not the case for systems that become disk-dominated which, in general, show coherence in the alignment of the spin axis. In these cases, the enclosed specific angular momentum increases roughly linearly with enclosed mass fraction. As Fig. 8 shows, the same result applies to all galaxies in our sample: despite the large scatter, on average, the degree of alignment at turnaround increases gradually with the importance of the disk component in the morphology of a galaxy at  $z = 0$ .

The right panels in Fig. 7 show that a similar assessment applies to the dark matter halo surrounding these galaxies. The halos of spheroids also show, at turnaround, stronger misalignments than the halos that host disk galaxies at  $z = 0$ . This is encouraging, since it implies that it might be possible to use the angular momentum properties of a dark matter halo at turnaround to “predict” the morphology of its central galaxy at  $z = 0$ . We emphasize, however, that the trends we highlight here, although well defined, are relatively weak, so the correspondence between early halo properties and final galaxy morphology is likely to apply statistically rather than to individual systems.

Quantitatively, the dependence of present day morphology on spin alignment at turnaround is shown in the inset panel of Fig. 8. Here we show, for each individual system,  $\kappa_{\text{rot}}$  versus the average cosine of the angle between the angular momentum enclosed by different mass shells and the total. The trend is clear: systems with better-aligned spins at turnaround tend to be more disk-dominated at present. The trend is even stronger when considering only systems where mergers have played a minor role ( $f_{\text{acc}} < 0.1$ , solid points). The correlation coefficient is  $r_s = 0.49$  (with significance  $\Delta \sim 2. \times 10^{-6}$ ) and confirms our earlier conclusion that significant misalignment in the distribution of angular momentum can lead to the formation of spheroid-dominated systems in the absence of significant merger events.

## 5 SUMMARY

We use gasdynamical cosmological simulations of galaxy formation to study the origin of different galaxy morphologies in the  $\Lambda$ CDM cosmogony at redshift  $z = 0$ . The GIMIC simulation series covers a large volume and has a resolution high enough to study the structure and kinematics of the stellar components of 100 central galaxies in Milky Way-sized halos. We focus our analysis on the origin of galaxy morphology, somewhat narrowly defined as the relative importance of rotational support vs velocity-dispersion support (the disk-to-spheroid ratio) in the structure of the galaxy. Our main results may be summarized as follows:

- The simulated galaxies span a wide range of morphological types, from rotation-free spheroids to almost pure disk galaxies where fewer than 5% of all stars are in counterrotating orbits. Disks have roughly exponential stellar surface density profiles and flat rotation curves, whereas spheroids are dense stellar systems that can be approximated by de Vaucouleurs’  $R^{1/4}$  profiles. The resemblance with real galaxies suggests that it should be possible to gain insight into the origin of galaxy morphology by studying the

mechanisms responsible for the relative importance of disks and spheroids in GIMIC galaxies.

- The morphology of simulated galaxies seems mostly unrelated to the spin or assembly history of their surrounding dark matter halos. Most stars form *in-situ* and comprise on average only about  $\sim 40\%$  of all available baryons in the halo. Such low galaxy formation “efficiency” may explain the weak correlation between the properties of halos and those of the central galaxy. Contrary to simple expectations, disks form in halos with low and high angular momenta, and spheroids form even in galaxies where most stars form *in-situ*, suggesting a formation path for spheroids that does not rely on merging.

- The star formation history provides an interesting clue to the origin of morphology. Disks tend to form gradually over long periods of time, whereas star formation in spheroids proceeds episodically, leaving behind populations of stars of similar age but distinct kinematics. These populations originate from the accretion of gas whose angular momentum is misaligned relative to that of earlier-accreted material. The misalignment destabilizes any pre-existing disk, prompts the rapid transformation of gas into stars, and reduces the net rotational support of the system.

- Misaligned accretion is reduced when the gas is shock-heated to a hot, pressure-supported corona before accretion. Gradual cooling from such a slowly-rotating corona thus favours the formation of disks. On the other hand, direct filamentary accretion of cold gas is often accompanied by substantial misalignment and favours the formation of spheroids.

- Since angular momentum is largely acquired at the time of maximum expansion of the material destined to form a galaxy, it follows that the present-day morphology of simulated galaxies is imprinted early, well before the assembly of the galaxy. Indeed, a good indicator of morphology at  $z = 0$  is the coherence in the alignment of the net spin of various parts of the system at the time of turnaround. Spheroid-dominated galaxies form in systems where misalignments are substantial whereas disks form in systems where the angular momentum of all mass shells is roughly aligned.

Our results suggest a new scenario for the origin of stellar spheroids that does not rely on merging. This scenario, once developed more thoroughly, should offer a number of predictions falsifiable by observation. For example, the episodic nature of star formation in spheroids envisioned here is expected to leave behind overlapping populations of stars of distinct age, kinematics, and, possibly, metallicity) that survive to the present because of the paucity of mergers. We plan to explore the observational signatures of these populations in future work.

The scenario we propose here also offers clues to the origin of pure disk, “bulgeless”, galaxies. Indeed, a number of our simulated galaxies are effectively bulgeless, and form either in systems where spin alignment is extraordinarily coherent or where most of the baryons in the galaxy get accreted late from a hot corona. The abundance of bulgeless galaxies depends strongly on galaxy mass (Fisher & Drory 2011; Fontanot et al. 2011); the narrow range in halo mass we consider here precludes a more quantitative investigation of these intriguing clues at this point.

Although coherent spin alignment at early times is clearly an important clue, it should be considered as one ingredient of the complex process that determines the morphology of a galaxy. Strong feedback, for example, may expel baryons from galaxies and cycle them through a hot corona before they get re-accreted and turned into stars, potentially erasing the spin alignment dependence we report here. Furthermore, aligned spins in the accreting

gas might not be enough to ensure the survival of a stellar disk, especially if the dark matter halo is strongly triaxial and its principal axes are not coincident with the disk. Finally, although mergers are rare in the mass range we explore here, they likely play a more important role in the formation of more massive spheroids. Until simulations can reproduce not only the properties of individual systems, but the full statistical distribution of galaxy morphologies and their dependence on mass and environment, it is likely that a full understanding of the origin of galaxy morphology will remain beyond reach.

## ACKNOWLEDGEMENTS

We thank Ian McCarthy for his contribution to the simulations used in this work, which were run at the Darwin HPC of Cambridge University. LVS is grateful for financial support from the CosmoComp/Marie Curie network. CSF acknowledges a Royal Society Wolfson research merit award and ERC Advanced Investigator grant COSMIWAY. This work was supported in part by an STFC rolling grant to the ICC.

## REFERENCES

- Abadi M. G., Navarro J. F., Steinmetz M., Eke V. R., 2003, *ApJ*, 591, 499
- Agertz O., Teyssier R., Moore B., 2011, *MNRAS*, 410, 1391
- Bett P. E., Frenk C. S., 2011, ArXiv e-prints 1104.0935
- Bournaud F., Chapon D., Teyssier R., Powell L. C., Elmegreen B. G., Elmegreen D. M., Duc P.-A., Contini T., Epinat B., Shapiro K. L., 2011, *ApJ*, 730, 4
- Bower R. G., Benson A. J., Malbon R., Helly J. C., Frenk C. S., Baugh C. M., Cole S., Lacey C. G., 2006, *MNRAS*, p. 659
- Brook C. B., Governato F., Quinn T., Wadsley J., Brooks A. M., Willman B., Stilp A., Jonsson P., 2008, *ApJ*, 689, 678
- Brook C. B., Governato F., Roškar R., Stinson G., Brooks A. M., Wadsley J., Quinn T., Gibson B. K., Snaith O., Pilkington K., House E., Pontzen A., 2011, *MNRAS*, 415, 1051
- Brooks A. M., Governato F., Quinn T., Brook C. B., Wadsley J., 2009, *ApJ*, 694, 396
- Bullock J. S., Dekel A., Kolatt T. S., Kravtsov A. V., Klypin A. A., Porciani C., Primack J. R., 2001, *ApJ*, 555, 240
- Bundy K., Treu T., Ellis R. S., 2007, *ApJL*, 665, L5
- Catelan P., Theuns T., 1996, *MNRAS*, 282, 436
- Cen R., Chisari N. E., 2011, *ApJ*, 731, 11
- Ceverino D., Klypin A., 2009, *ApJ*, 695, 292
- Chabrier G., 2003, *ApJL*, 586, L133
- Christodoulou D. M., Shlosman I., Tohline J. E., 1995, *ApJ*, 443, 551
- Cole S., Lacey C. G., Baugh C. M., Frenk C. S., 2000, *MNRAS*, 319, 168
- Crain R. A., McCarthy I. G., Frenk C. S., Theuns T., Schaye J., 2010, *MNRAS*, 407, 1403
- Crain R. A., Theuns T., Dalla Vecchia C., Eke V. R., Frenk C. S., Jenkins A., Kay S. T., Peacock J. A., Pearce F. R., Schaye J., Springel V., Thomas P. A., White S. D. M., Wiersma R. P. C., 2009, *MNRAS*, 399, 1773
- Croft R. A. C., Di Matteo T., Springel V., Hernquist L., 2009, *MNRAS*, 400, 43

- Croton D. J., Springel V., White S. D. M., De Lucia G., Frenk C. S., Gao L., Jenkins A., Kauffmann G., Navarro J. F., Yoshida N., 2006, *MNRAS*, 365, 11
- Dalla Vecchia C., Schaye J., 2008, *MNRAS*, 387, 1431
- De Lucia G., Fontanot F., Wilman D., Monaco P., 2011, *MNRAS*, 414, 1439
- Dekel A., Birnboim Y., 2006, *MNRAS*, 368, 2
- Dekel A., Sari R., Ceverino D., 2009, *ApJ*, 703, 785
- Dolag K., Borgani S., Murante G., Springel V., 2009, *MNRAS*, 399, 497
- Efstathiou G., Lake G., Negroponte J., 1982, *MNRAS*, 199, 1069
- Eggen O. J., Lynden-Bell D., Sandage A. R., 1962, *ApJ*, 136, 748
- Fall S. M., Efstathiou G., 1980, *MNRAS*, 193, 189
- Fisher D. B., Drory N., 2011, *ApJL*, 733, L47
- Font A. S., McCarthy I. G., Crain R. A., Theuns T., Schaye J., Wiersma R. P. C., Dalla Vecchia C., 2011, *MNRAS*, 416, 2802
- Fontanot F., De Lucia G., Wilman D., Monaco P., 2011, *MNRAS*, 416, 409
- Frenk C. S., White S. D. M., Efstathiou G., Davis M., 1985, *Nature*, 317, 595
- Governato F., Brook C. B., Brooks A. M., Mayer L., Willman B., Jonsson P., Stilp A. M., Pope L., Christensen C., Wadsley J., Quinn T., 2009, *MNRAS*, 398, 312
- Governato F., Willman B., Mayer L., Brooks A., Stinson G., Valenzuela O., Wadsley J., Quinn T., 2007, *MNRAS*, 374, 1479
- Haardt F., Madau P., 2001, in D. M. Neumann & J. T. V. Tran ed., *Clusters of Galaxies and the High Redshift Universe Observed in X-rays Modelling the UV/X-ray cosmic background with CUBA*
- Hahn O., Teyssier R., Carollo C. M., 2010, *MNRAS*, 405, 274
- Hopkins P. F., Bundy K., Croton D., Hernquist L., Keres D., Khochfar S., Stewart K., Wetzel A., Younger J. D., 2010, *ApJ*, 715, 202
- Hubble E. P., 1926, *ApJ*, 64, 321
- Kennicutt Jr. R. C., 1989, *ApJ*, 344, 685
- Kennicutt Jr. R. C., 1998, *ARA&A*, 36, 189
- Kereš D., Katz N., Weinberg D. H., Davé R., 2005, *MNRAS*, 363, 2
- Larson R. B., 1974, *MNRAS*, 166, 585
- Larson R. B., 1976, *MNRAS*, 176, 31
- McCarthy I. G., Font A. S., Crain R. A., Deason A. J., Schaye J., Theuns T., 2011, *ArXiv e-prints* 1111.1747
- Meza A., Navarro J. F., Steinmetz M., Eke V. R., 2003, *ApJ*, 590, 619
- Mo H. J., Mao S., White S. D. M., 1998, *MNRAS*, 295, 319
- Navarro J. F., Frenk C. S., White S. D. M., 1995, *MNRAS*, 275, 56
- Navarro J. F., Hayashi E., Power C., Jenkins A. R., Frenk C. S., White S. D. M., Springel V., Stadel J., Quinn T. R., 2004, *MNRAS*, 349, 1039
- Navarro J. F., Steinmetz M., 1997, *ApJ*, 478, 13
- Oesch P. A., Carollo C. M., Feldmann R., Hahn O., Lilly S. J., Sargent M. T., Scarlata C., 24 coauthors 2010, *ApJL*, 714, L47
- Okamoto T., Eke V. R., Frenk C. S., Jenkins A., 2005, *MNRAS*, 363, 1299
- Parry O. H., Eke V. R., Frenk C. S., 2009, *MNRAS*, 396, 1972
- Partridge R. B., Peebles P. J. E., 1967, *ApJ*, 147, 868
- Piontek F., Steinmetz M., 2011, *MNRAS*, 410, 2625
- Porciani C., Dekel A., Hoffman Y., 2002a, *MNRAS*, 332, 325
- Porciani C., Dekel A., Hoffman Y., 2002b, *MNRAS*, 332, 339
- Power C., Navarro J. F., Jenkins A., Frenk C. S., White S. D. M., Springel V., Stadel J., Quinn T., 2003, *MNRAS*, 338, 14
- Robertson B., Bullock J. S., Cox T. J., Di Matteo T., Hernquist L., Springel V., Yoshida N., 2006, *ApJ*, 645, 986
- Sales L. V., Navarro J. F., Schaye J., Dalla Vecchia C., Springel V., Booth C. M., 2010, *MNRAS*, 409, 1541
- Sales L. V., Navarro J. F., Schaye J., Dalla Vecchia C., Springel V., Haas M. R., Helmi A., 2009, *MNRAS*, 399, L64
- Scannapieco C., Gadotti D. A., Jonsson P., White S. D. M., 2010, *MNRAS*, 407, L41
- Scannapieco C., Tissera P. B., White S. D. M., Springel V., 2008, *MNRAS*, 389, 1137
- Scannapieco C., White S. D. M., Springel V., Tissera P. B., 2009, *MNRAS*, 396, 696
- Schaye J., Dalla Vecchia C., 2008, *MNRAS*, 383, 1210
- Schaye J., Dalla Vecchia C., Booth C. M., Wiersma R. P. C., Theuns T., Haas M. R., Bertone S., Duffy A. R., McCarthy I. G., van de Voort F., 2010, *MNRAS*, 402, 1536
- Somerville R. S., Barden M., Rix H.-W., Bell E. F., Beckwith S. V. W., Borch A., Caldwell J. A. R., Häußler B., Heymans C., Jahnke K., Jøgee S., McIntosh D. H., Meisenheimer K., Peng C. Y., Sánchez S. F., Wisotzki L., Wolf C., 2008, *ApJ*, 672, 776
- Springel V., 2005, *MNRAS*, 364, 1105
- Springel V., White S. D. M., Jenkins A., Frenk C. S., Yoshida N., Gao L., Navarro J., Thacker R., Croton D., Helly J., Peacock J. A., Cole S., Thomas P., Couchman H., Evrard A., Colberg J., Pearce F., 2005, *Nature*, 435, 629
- Springel V., Yoshida N., White S. D. M., 2001, *New Astronomy*, 6, 79
- Steinmetz M., Navarro J. F., 2002, *New Astronomy*, 7, 155
- Toomre A., 1977, in Tinsley B. M., Larson R. B., eds, *Evolution of Galaxies and Stellar Populations Mergers and Some Consequences*. p. 401
- van de Voort F., Schaye J., Booth C. M., Haas M. R., Dalla Vecchia C., 2011, *MNRAS*, 414, 2458
- Vogelsberger M., Sijacki D., Keres D., Springel V., Hernquist L., 2011, *ArXiv e-prints* 1109.1281
- White S. D. M., 1984, *ApJ*, 286, 38
- White S. D. M., Frenk C. S., 1991, *ApJ*, 379, 52
- White S. D. M., Rees M. J., 1978, *MNRAS*, 183, 341
- Wiersma R. P. C., Schaye J., Smith B. D., 2009, *MNRAS*, 393, 99
- Wiersma R. P. C., Schaye J., Theuns T., Dalla Vecchia C., Tornatore L., 2009, *MNRAS*, 399, 574
- Zavala J., Okamoto T., Frenk C. S., 2008, *MNRAS*, 387, 364